Design of a prompt-gamma neutron activation analysis system on China Advanced Research Reactor

SUN Hongchao[1,*] NI Bangfa[1] XIAO Caijin[1] ZHANG Guiying[1]
LIU Cunxiong[1] HUANG Jinfeng[2]

[1]*China Institute of Atomic Energy, Beijing 102413, China*

[2]*GuangXi University, Guangxi 530004, China*

Abstract In this paper, computational methods are used to optimize the design of a prompt-gamma neutron activation analysis (PGNAA) system on China Advanced Research Reactor (CARR). Approaches are adopted for obtaining accurate neutron beam parameter and saving the computing time. For the radiation shielding design, the optimizing factors include the cost, weight, volume, machining convenience and background radiation at the detector position. Low background spectrum and high sensitivity are expected. The simulation results, and experiences from international PGNAA community, were used in the design of the CARR PGNAA system.

Key words Prompt gamma activation analysis, PGAA Facility, Neutron Cross-section, Shielding

1 Introduction

Prompt-gamma neutron activation analysis (PGNAA) is a nondestructive method for high sensitive multi-elemental analysis, with an increasing range of applications in over 30 PGNAA facilities worldwide[1,2]. A PGNAA facility is being set up on the China Advanced Research Reactor (CARR) at China Institute of Atomic Energy. The CARR is a 60-MW tank-in-pool reactor of inverse neutron trap-type. Light water is used as moderator and primary cooling. The reactor core is surrounded by heavy water reflector, where the maximum unperturbed thermal neutron flux is estimated at 8×10^{14} $cm^{-2}\cdot s^{-1}$ at 60 MW. Among its nine tangent horizontal beam tubes, the HT2# is being used for PGNAA, apart from its vertical tubes in both the reflector and pool for different applications.

Extracted by the HT2# beam tube 46 cm from the reactor core, the neutrons can be of a normalized flux of 10^9 $cm^{-2}\cdot s^{-1}$ at the HT2# outlet after they transmit through the collimators and the mono-crystal Bi filter. Cross section of the neutron beam is 2.5 cm×2.5 cm at the outlet, which is resized by an outer collimator. Fig.1 is schematics of the PGNAA facility consisting of the collimators, a sample chamber, detection equipment, beam stopper and beam tube.

The beam tube and chamber is evacuated, so as to reduce the number of neutrons scattered by the air. The detection system consists of a germanium detector and bismuth germanate (BGO) Compton suppressor, which suppresses unwanted peaks and continuous background and thereby increases analysis sensitivity and selectivity. The shielding materials are selected based on weight, cost, volume, and machining convenience. The sizes are optimized by simulations, aiming at good radiation protection and low gamma background. The CARR shall be one of the research reactors with the highest neutron fluxes[3-6], and the PGNAA system will be set up at a high level.

MCNP is a general purpose Monte Carlo N-particle code which can be used for neutron, photon, and electron or coupled neutron/photon/electron transport, being capable of calculating eigen values for critical systems. It treats an arbitrary three dimensional configuration of materials in geometric cells bounded

Supported by National Natural Science Foundation of China (No.10805077)
* Corresponding author. *E-mail address:* hcsun@ciae.ac.cn
Received date: 2011-06-22

by first and second degree surfaces and fourth degree elliptical tori. MCNP−4B[7] program was released in 1997. In this paper, we use this code, and its ENDF/B−VI based continuous-energy cross-section library, to optimize the CARR PGNAA design.

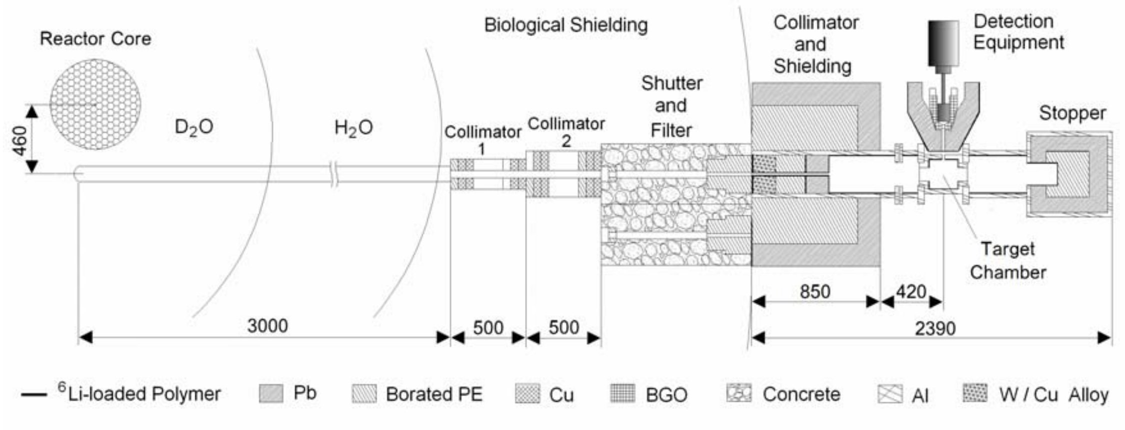

Fig.1 Schematics of the PGNAA system on CARR.

2 Simulation

2.1 General description

The MC simulations were performed with subsection method[8], which saves computer hours for especially complicated facility geometry and long range particle-transportation. The simulations were done on two sections of the design: 1) from the entryway of HT2# to its outlet; and 2) from collimator 1 to the stopper. For an ideal transition between the two sections, section 2 begins from collimator 1 rather than the HT2# outlet, and the distance between the collimator 1 and the HT2# outlet is 2 m.

The surface source of section 1 was defined cross-section of the HT2# entrance, where the neutron flux was 2.3674×10^{16} s^{-1}, and the energy spectrum and direction spectrum had been obtained. Tally type 1 was used to record the current, energy spectrum, spatial distributing and direction spectrum of the neutron beam, through the HT2# cross-section at collimator 1, which was defined as the surface source of section 2, where the normalized neutron flux was 2.1438×10^{14} s^{-1}. Tally type 1 and 2 were used to record the flux of γ-rays and neutrons transmission through the surfaces of interest. For accurate simulations, the neutron beam parameters were corrected (see Section 2.2), and γ-rays from the reactor core were solely simulated.

2.2 Filtering of the fast neutrons

Mono-crystalline Bi is used to filter the fast neutrons, of which the total cross-section σ_t is given as

$$\sigma_t = \sigma_a + \sigma_{TDS} + \sigma_{Bragg} \tag{1}$$

where, σ_a is the absorption cross-section, σ_{TDS} is the thermal diffuse cross-section, and σ_{Bragg} is the Bragg scattering cross-section. σ_a can be written as

$$\sigma_a = C_1 E^{-1/2} \tag{2}$$

where, E is the neutron energy and $C_1=\sigma_0 E_0^{1/2}$ (σ_0 and E_0 can be obtained from Ref.[9]).

According to Freund[10], σ_{TDS} is given by

$$\sigma_{TDS} = [A/(A+1)]^2 + \sigma_{bat} + [1 - e^{-(B_0+B_T)C_2E}] + \frac{\theta_D^{1/2}\sigma_{bat}}{36AE^{1/2}}\begin{cases} R \rightarrow x \le 6, \\ 3.3x^{-7} \rightarrow x \ge 6, \end{cases} \tag{3}$$

where, $x=\theta_D/T$, θ_D is the characteristic Debye temperature, T is the sample temperature; $\sigma_{bat}=S+s$, S and s are coherent and incoherent scattering cross-section of the bound atom, respectively; $A=209$ is atomic mass number of Bi, C_2 is a constant independent of scattering material, $B_0=3h^2/(2K_B\theta_D A)$, corresponds to the zero-point motion and is temperature-independent, h is the Plank constant, and K_B is the Boltzman coefficient. The series $R=\sum B_n X^{n-1}/[n!(n+5/2)]$, where B_n is the Bernoulli numbers. The temperature-dependence is given by

$$B_{\mathrm{T}} = 4B_0\phi(x)/x$$

$$\phi(x) = x^{-1}\int_0^x \xi d\xi/(e^{-\xi}-1) \tag{4}$$

According to M.Adib[11], σ_{Bragg} of mono-crystalline Bi is

$$\sigma_{\mathrm{Bragg}} = \frac{1}{Nt_0}\ln\left(\frac{1}{T_{\mathrm{Bragg}}}\right) \tag{5}$$

where N is the number of atoms/cm^3, and t_0 is the effective thickness in cm of the crystal. The neutron transmission from different planes (hkl) is given by

$$T_{\mathrm{Bragg}} = \Pi(1-P_{hkl}{}^{\theta}) \tag{6}$$

where $P^{\theta}{}_{hkl}$ is the reflecting power of (hkl) plane of mono-crystalline Bi inclined by an angle θ_{hkl} to the beam incidence. According to Bacon[12], the reflecting power is given by

$$P^{\theta}_{\mathrm{hkl}} = \frac{Q_{\mathrm{hkl}}t_0}{\gamma_0}\frac{W(\theta-\theta_{\mathrm{B}})}{1+Q_{\mathrm{hkl}}t_0/[W(\theta-\theta_{\mathrm{B}})\gamma_0]} \tag{7}$$

where Q_{hkl} is the Q-value of the crystal at the (hkl) plane given by

$$Q_{\mathrm{hkl}} = \frac{\lambda^3 N_{\mathrm{c}}{}^2}{\sin(2\theta)}F^2_{\mathrm{hkl}}e^{-2\mathrm{W}} \tag{8}$$

where N_{c} is the number of unit cells per unit volume, γ_0 is the direction cosine of the incident beam relative to the inward normal to the crystal face cutting along the ($h_{\mathrm{c}}k_{\mathrm{c}}l_{\mathrm{c}}$) plane, and η is the standard deviation of the mosaic blocks. $W(\Delta)$ is the angular distribution of the mosaic blocks,

$$W(\Delta) = {}^{1}\!/_{\eta\sqrt{2\pi}}\, e^{-\Delta^2/2\eta^2} \tag{9}$$

where F_{hkl} is the structure factor of the (hkl) plane and $e^{-2\mathrm{W}}$ is the Debye correction factor. For the hexagonal close-packed structure (*HCP*), the glancing angle θ and the Bragg angle θ_{B} for the (hkl) plane can be calculated according to M.Adib[11].

A program in Matlab language was written to calculate the total thermal cross-section of mono-crystalline Bi using Eq.(1), in the energy range of 10^{-4} eV<E<10 eV, as curve (b) in Fig.2. as the data of θ_{D}, σ_{bat}, C_2, F_{hkl}, N, N_{c}, etc. were obtained from Refs.[10,11]. A Bi crystal cut along the [111] plane has a thermal neutron window[10], hence a good filter of fast neutrons.

In fact, the free-atom neutron cross-sections for Bi are used in the library of ENDF601 (from ENDF/B-VI[13]) released with MCNP[7], as curve (a) in Fig.2, which is not in accord with the neutron cross sections for mono-crystalline Bi. Fig.3 is the simulation results of MCNP. Comparing the neutron spectrum at the HT2# outlet with Bi filter using free atom cross-section (○) to that at the source (Δ), one sees no filtering effect but finds that the (○) spectrum is much harder than the (Δ) spectrum. Therefore, the beam parameters were corrected by Eq.(1), in the energy range 10^{-4} eV $<E<10$ eV, and the improved neutron spectrum at the HT2# outlet (□) has a flux of about 10^9 cm^{-2}·s^{-1}. Fig.3 shows also the neutron spectrum at the HT2# outlet without any filter (◊), indicating the need of a filter to obtain thermal neutrons.

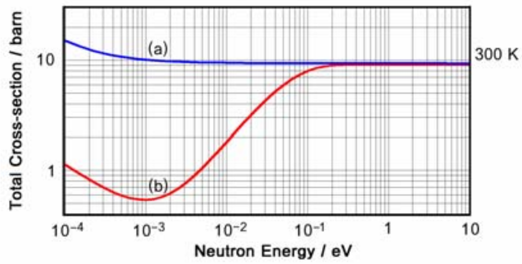

Fig.2 Total thermal cross-section of mono-crystalline Bi. (a) free gas model and (b) by Eq.(1).

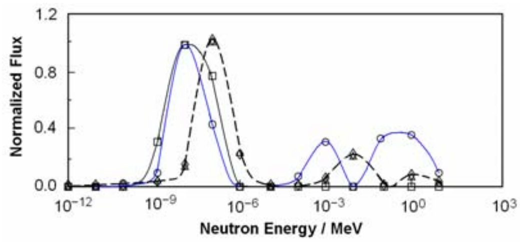

Fig.3 Neutron spectra at the source (Δ), and at the HT2# outlet without filter (◊) and with Bi filter using free atom cross-section (○) and the cross-section calculated by Eq.(1) (□).

2.3 Radiation shielding

The radiation shielding shall meet the requirements of radiation protection and low gamma background. Factors for optimizing the radiation shielding design covered the weight, volume, machining convenience, cost and low background at the detector position. Materials used for the radiation shielding included borated polyethylene, ^{6}Li-loaded polymer, W/Cu alloy, lead, bismuth and aluminum.

Borated polyethylene, being easy to machine and having high cross-section of neutron absorption, was used for neutron shielding. A few millimeter thick

^{6}Li-loaded polymer can capture the vast majority of thermal neutrons, hence its use as a lining of the collimator, stopper recess and beam tube. Tungsten/copper alloy was used in front part of the collimators, so as to reduce the neutron energy by inelastic scattering. Lead and bismuth were used for shielding γ-rays. Aluminum is a suitable material to support the equipment.

3 Design of the PGNAA system

Designing the PGNAA parts was based on the MCNP simulation results and experiences from international PGNAA community. The detailed designs are as follows:

3.1 Collimator

A collimator is 51.20-cm long with a 1.5 cm×1.5 cm aperture lined with ^{6}Li-loaded polymer. It consists of 0.4-cm thick ^{6}Li-loaded polymer, 15-cm thick W/Cu alloy, 20-cm borated PE, 0.4-cm thick ^{6}Li-loaded polymer and 15-cm thick lead, in sequence of the beam incidence.

To make the PGNAA system applicable for larger volume sample, a collimator with 2.5 cm×2.5 cm aperture was designed. Besides, we are to design a device which can circumrotate a larger sample and analyze each point of the sample.

The outside shielding of collimator is 85-cm long, with 30-cm thick borated polyethylene surrounded by 15-cm thick lead. The MCNP simulation results show that γ-rays and neutrons escaped from the shielding surface are just 58 $\gamma\cdot cm^{-2}\cdot s^{-1}$ and 72 $n\cdot cm^{-2}\cdot s^{-1}$, respectively.

3.2 Sample chamber

The sample chamber is a 20-cm sided cubic cavum, lined with ^{6}Li-loaded polymer. Neutron beam passes the chamber through the Φ9 cm entrance and outlet. A cylindrical recess, cut into the side of the chamber facing the detector, accommodates a piece of thin magnesium alloy.

3.3 Detection equipment

The detection system consists of a Ge detector and a BGO Compton suppressor, surrounded by 10-cm thick lead, which is in turn surrounded by a shell of ^{6}Li-loaded polymer. Besides, a layer of ^{6}Li-loaded polymer is placed between the sample and detectors, which can shield 90% neutrons, scattered by the sample and allow the passage of γ-rays. The BGO suppresses unwanted peaks and continuous background, hence the increase of analysis sensitivity and selectivity. The prompt γ-rays from the sample reach the detector through a Φ2 cm×10 cm lead collimator. The sample to detector distance is 27.5 cm, which is large enough to minimize the effect of peak summing.

3.4 Beam stopper

The beam stopper is a Φ14.4 cm×20 cm cylindrical recess lined with ^{6}Li-loaded polymer to eliminate low energy component of the neutron beam. The cylindrical recess is a 30-cm sided borated polyethylene cubes surrounded by 10-cm thick lead. The simulation shows that γ-rays and neutrons escaped from the shielding surface are just 69 $\gamma\cdot cm^{-2}\cdot s^{-1}$ and 22 $n\cdot cm^{-2}\cdot s^{-1}$, respectively.

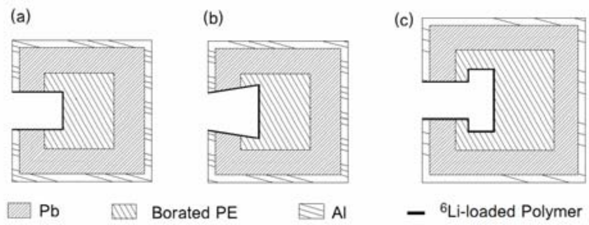

Fig.4 Stoppers with a cylindrical recess (a), a truncated cone recess (b) or a cavum (c).

Of the three types of beam stopper in Fig.4, stopper (c) should have the least contribution to background in theory, which is confirmed by the MCNP simulation. On cross-section of the beam tube 30-cm away from the stopper, the intensities of γ-rays back-reflected from the stopper are 20, 21 and 15 $\gamma\cdot cm^{-2}\cdot s^{-1}$ for beam stoppers (a), (b) and (c), respectively. However, because of the large recess of stopper (c), we would have to enlarge the volume, plus thick enough shielding materials on each side, for reducing the γ-rays and neutrons escaping from the stopper surface. As a result of comprehensive considerations on the weight, volume, cost and the background, type (a) stopper was finally selected.

3.5 Beam tube

The beam tube is a 26-cm (ID) aluminum pipe lined with ^{6}Li-loaded polymer. In order to minimize the number of neutrons scattered by the air, the tube can be evacuated or filled with He. It is of a front part of 100 cm and a back part of 70 cm. Such a scheme ensures the reasonable distances between the HT2$^\#$ outlet and target chamber, and between the chamber and stopper.

Low background spectrum and high sensitivity are essential requirements for a PGNAA system. The largest sources of γ-rays are from the stopper and beam entry. Some nuclides in the structural materials may be activated by neutrons and emit γ-rays. To minimize their contribution to the background, the tube is lined with ^{6}Li-loaded polymer to decrease the number of nuclides in the structural materials to be activated by neutrons, the target chamber-stopper distance was increased to reduce γ-rays reflected from the stopper, the tube and chamber are evacuated to minimize the number of air-scattered neutrons, and Bi is used to filter γ-rays from the reactor core.

The MCNP simulation was performed first with the neutron beam passing through an empty target chamber. The results showed that the γ-rays detected was 174 cps (assuming a 100% detection efficiency), indicating that the gamma background is mostly caused by the activated nuclides in the structural materials. Then, a second simulation was done on the chamber with a D_2O sample, which scatters neutrons at the target position, and the γ-rays detected were of 801 cps, roughly 4 times higher than that of the empty chamber. This is due to that the neutrons scattered by the D_2O sample induce activation of the structural materials.

Also, the simulation showed that γ-rays from the reactor core were of 1.1×10^6 $cm^{-2}\cdot s^{-1}$at the target position. This is a little higher because the free atom mode for Bi was used in the MCNP, but this is a small contribution to the gamma background. During the MCNP simulation, the BGO Compton suppressor was not included in the physical models. Some actual measurements, as the spectrum of room-background or the Compton suppressed background spectrum, will be performed after establishment of the PGNAA system.

4 Conclusion

The free-atom neutron cross-sections for bismuth, which are used in MCNP, are not suitable for simulating mono-crystalline Bi. Eq.(1) was therefore used in the correction of beam parameters after the neutron transmission through mono-crystalline Bi. The radiation shielding was optimized with regard to the weight, volume, machining convenience, cost and the effectiveness in lowering the background at the detector position. The subsection method[8], which saves computer hours, was adopted in the design. The simulation results show that the design meets the requirements of radiation protection, with low gamma background and high sensitivity.

The HT2$^\#$ shutter has three apertures, and different filter materials of mono-crystalline Bi, ^{56}Fe, Sc, mono-crystalline silicon, sapphire, uranium etc. will be mounted to select different neutron spectra for various applications[14,15]. Thermal neutron beam obtained using mono- crystalline Bi filter is widely applied in PGNAA. The 24 and 2 keV quasi-single energy neutron beams respectively obtained using ^{56}Fe and Sc filters can be applied to nuclear structure studies, such as 24-keV neutron capture studies and resonant neutron capture studies[16-18].

References

1 Paul R L, Lindstrom R M, Brucker C, *et al.* J Radioanal Nucl Chem, 2000, **243:** 181−189.

2 Choi D, Sun G M, Byun S H. The 2nd Meeting of the IAEA CRP on PGNAA[C]. Vienna: IAEA, 2001, 29−32.

3 Choi H D, Byun S H. 2000 workshop on the Utilization of Research Reactor Nov 20−24, Korea, 2000.

4 Revay Z, Belgya T, Kasztovszky Z, *et al.* Nucl Instrum Meth A, 2004, **213:** 385−388.

5 Paul R L, Lindstrom R M, Heald A E. J Radioanal Chem, 1997, **215:** 63−68.

6 Crittin M, Kern J, Schenker J L. Nucl Instrum Meth A, 2000, **449:** 221−236.

7 Briesmeister J F (Ed.). MCNP−A General Monte Carlo N-Particle Transport Code, version 4B, LA−12625−M, Los Alamos National Laboratory, 1997.

8 Zhong Z P, Shi G, Hu Y M. J Tsinghua Univ (Sci & Tech), 2001, **41:** 16−20 (in Chinese).

9 Sears V F. Neutron News, 1992, **3:** 26−37.

10 Freund A K. Nucl Instrum Meth, 1983, **213:** 495−501.

11 Adib M, Kilany M. Radiat Phys Chem, 2003, **66:** 81−88.
12 Bacon G E. Neutron Diffraction 3rd edn. Oxford: Clarendon, 1975.
13 Rose P E, Compiler and Editor. “ENDF-201, ENDF/B−VI Summary Documentation,” BNLNCS−17541, Brookhaven National Laboratory, 1991.
14 Greenwood R C, Reich C W. Phys Rev C, 1971, **4:** 2249−2255.
15 Gritzay O, Kolotyi V, Klimova N, *et al.* International Conference on nuclear Data for Science and Technology 2007.DOI:10.1051/ndata:07228.
16 Gritzay O, Kolotyi V, Pshenichnyi V, *et al.* 6th Conference on Nuclear and Particle Physics, Luxcor, Egypt, 17−21 Nov., 2007.
17 Rimawi K, Chrien R E. Phys Rev C, 1977, **15:** 1271−1281.
18 Egidy T V, Cizewski J A, McCullagh C M, *et al.* Phys Rev C, 1979, **20:** 944−955.